JGR Oceans

RESEARCH ARTICLE
10.1029/2018JC014870

A Scaling for Wave Dispersion Relationships in Ice-Covered Waters

Jie Yu[1], **W. Erick Rogers**[1], **and David W. Wang**[1]

[1]Naval Research Laboratory, Stennis Space Center, MS, USA

Key Points:
- A simple scaling of dispersion relations is proposed and shown to be effective
- Dimensionless parameters are identified, which can guide the similarity of wave propagation under ice
- The method results in scale collapse of data and more consistent estimates of effective ice properties

Supporting Information:
- Supporting Information S1

Correspondence to:
J. Yu,
Jie.Yu@nrlssc.navy.mil

Citation:
Yu, J., Rogers, W. E., & Wang, D. W. (2019). A scaling for wave dispersion relationships in ice-covered waters. *Journal of Geophysical Research: Oceans Oceans*, *124*, 8429–8438. https://doi.org/10.1029/2018JC014870

Received 14 DEC 2018
Accepted 4 NOV 2019
Accepted article online 22 NOV 2019
Published online 30 NOV 2019

Abstract We consider the scaling of dispersion relationships for wave propagation on ice-covered waters, aiming to identify a set of parameters that are physically meaningful and can be used in various continuum-based theories. These parameters characterize the relative importance of the effects of ice inertia, effective viscosity, and elasticity, hence can be used to guide the dynamic similarity between different scales. Application to laboratory and field measurements shows scale collapse of data sets toward a general trend. From the dimensionless parameters of the theoretical prediction, the effective ice properties can be estimated more consistently.

Plain Language Summary Sea ice covering the ocean surface, in the form of large sheets, floes, or slushy ice-water mixture, can modify the wavelength and dissipate the energy of ocean waves. Despite the difficulty of modeling the highly heterogeneous ice condition, various mathematical theories exist, describing the dependence of wavelength and dissipation on wave frequency under the effects of ice. These are called the wave dispersion relationships in ice-covered waters. In this paper, we consider a more efficient way to present various mathematical theories and compare them in a physically meaningful way. We find that the problem can be redefined in terms of nondimensional variables, which, to some extent, reconcile the apparent discrepancies between dissimilar laboratory and field data in the literature. The proposed nondimensionalization (scaling) also allows us to estimate the apparent viscosity and elasticity of the ice cover with better consistence. Nondimensional parameters are identified that characterize the relative importance of the apparent ice viscosity and elasticity, as well as ice inertia, by comparison. Therefore, they can guide the dynamical similarity of wave propagation under ice in different scales.

1. Introduction

In mathematical modeling, large ice sheets, floes, and the upper layer of water with floating pancake, brash, and frazil ice may be treated as a continuum with certain effective (rather than material) properties such as elasticity and viscosity (e.g., Mosig et al., 2015; Wang & Shen, 2010b). In this type of theory, the dispersion relationship is the first-order approximation that provides an estimate of the effects of ice on the wavelength (hence the wave speed), and the spatial attenuation rate of wave energy if the continuum ice is dissipative. Having a viable dispersion relationship is therefore crucial in field-scale modeling of waves in polar regions, since the wave speed, wavelength, and attenuation rate affect the various terms in the wave action equation that evolves the energy spectrum in space-time. Despite the immense advances in research, developing a realistic dispersion relationship remains challenging, in view of the heterogeneous condition of sea ice, especially in marginal ice zones.

At present, in operational wave models, for example, WAVEWATCH III® (The WAVEWATCH III Development Group, 2016), the effects of sea ice are optionally represented by a user-specified wave dispersion relationship. Various continuum-based theories are available in the literature, including the mass loading model (Weitz & Keller, 1950), the elastic plate model (e.g., Fox & Squire, 1994), the two-layer model of viscous ice-containing water overlying inviscid water (Keller, 1998; Weber, 1987) and its extension to the viscoelastic ice layer (Wang & Shen, 2010b), the model of two viscous fluids (De Carolis & Desiderio, 2002) , among others; see the reviews in Squire et al. (1995) and Squire (2007). There is little physics-based guidance to determine which theory is appropriate under what conditions, except for the obvious fact that nondissipative models such as the mass loading and pure elastic plate theories do not provide an estimate of wave attenuation rate. Determining the values of those effective ice properties is yet another nontrivial task, since they vary significantly depending on the ice condition.

On the other hand, measurements of wave attenuation rate and wavenumber are often analyzed in terms of dimensional variables (e.g., Hayes et al., 2007; Meylan et al., 2014; Rogers et al., 2016; Wadhams et al., 1988). With fewer exceptions (e.g., Newyear & Martin, 1997), comparisons of theories and data are also often made in dimensional planes (e.g., Cheng et al., 2017; Mosig et al., 2015; Wang & Shen, 2010a). The knowledge so acquired, such as curve fittings, agreements, or disagreements, tends to be limited to the conditions of individual data sets. A generalization would require a scaling law to guide the dynamic similitude. This is typically achieved through appropriate normalization using the scales that are physically relevant. As an illustration, consider the well-familiar dispersion relationship for waves on the open water, $\omega^2 = gk \tanh kd$, where ω is the angular frequency, k is the wavenumber, d is the water depth, and g is the gravitational acceleration. The water depth is clearly important to the wave propagation. Using d as the length scale, we write the dimensionless dispersion relationship $\hat{\omega}^2 = \hat{k} \tanh \hat{k}$, where $\hat{\omega} = \omega\sqrt{d/g}$ and $\hat{k} = kd$. In the dimensional plane, the dispersion relationship would be represented by different curves ω versus k according to different values of d, but upon normalization, all these curves collapse onto $\hat{\omega}$ versus $\hat{k}$. The scale collapse manifests the dynamic similarity of wave propagation: A longer wave in a deeper depth propagates similarly as a shorter wave in a shallower depth, if they have the same dimensionless frequency $\hat{\omega}$. (During the review of this paper, it was brought to our attention that some readers may regard the power laws of wave attenuation rate k_i (which can be treated as the imaginary part of the complex wavenumber in continuum-based theories of wave dispersion relationship, if the ice cover is dissipative) in Meylan et al. (2018) also as a scaling law. Meylan et al. (2018) explored empirical curve fittings in terms of dimensional variables, proposing $k_i \sim \omega^{3.27}$ or more precisely $k_i = \beta_1\omega^2 + \beta_2\omega^4$, based on observations. This type of empirical relationships is difficult to be generalized from one scale to another, since the fitting coefficients are dimensional and not physically explainable. That is different from the scaling to be studied in this paper.)

Whereas normalization is a straightforward mathematical process, identifying the dimensionless parameters that are of physical significance is the key. These parameters measure the relative importance of the physical processes involved and thus are able to ensure the dynamic similitude between cases of different scales. In this study, we shall explore the scaling of wave dispersion relationships in ice-covered waters, attempting to identify a set of parameters that are appropriate in this type of problem. In the domain of these dynamical parameters, theories can be classified into appropriate regimes according to their physical bases and meaningfully compared. Our purpose is not to develop a new theory, nor to review or assess the existing ones, but to demonstrate the effectiveness of scaling. To that end, we shall limit ourselves to a few commonly cited dispersion relationships, reexamining them in dimensionless form. We note that Keller (1998) discussed the results of viscous ice layer model, and its various limits, in terms of dimensionless variables and parameters. The Reynolds number in Keller (1998) is defined differently from the one used here (see section 2). Wang and Shen (2010b) mentioned normalization but did not identify the relevant parameters or to present the dimensionless results. While we do not claim that the simple scaling proposed here is definitive, or general, we will demonstrate that it does tend to collapse different data sets toward a general trend.

The rest of the paper is organized as follows. In section 2, we present the normalization of the selected wave dispersion relationships, unmasking the dynamical parameters. To show the relevance, in section 3 we reanalyze 8 laboratory data sets from various studies and 11 data sets from a recent field study, comparing the normalized data with the theoretical predictions. Conclusions follow in section 4.

2. Theoretical Models

The thickness of ice cover on the ocean surface inarguably plays an important role in wave-ice interaction. The water depth below becomes relatively unimportant, especially when it is deep as in open oceans. Using the thickness h of the ice layer as the scale for length, we define the dimensionless frequency and wavenumber:

$$\hat{\omega} = \omega\sqrt{h/g}, \quad \hat{k} = kh. \tag{1}$$

For $g = 9.83\text{m/s}^2$ in polar regions, $\hat{\omega} = 0.20$ corresponds to a 10-s wave under an ice layer of $h = 1$ m, or a 3.2-s wave under an ice layer of $h = 10$ cm. Without losing any generality and for mathematical simplicity, we shall consider the water depth d below the ice to be deep; that is, $\tanh kd \simeq 1$. Under the normalization (1), the open-water dispersion relationship is $\hat{k}_{\text{ow}} = \hat{\omega}^2$.

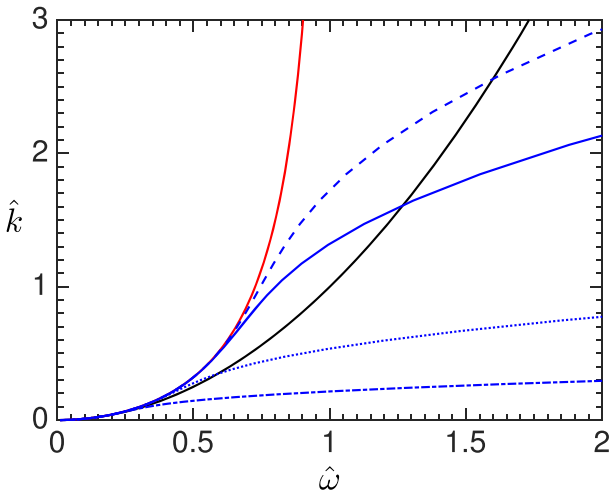

Figure 1. The dispersion relationships: mass loading model (red curve); the pure elasticity plate model (blue curves) with $\Gamma = 0.5$ (dashed), $\Gamma = 1$ (solid), $\Gamma = 10$ (dotted), and $\Gamma = 100$ (dash dotted). $\Pi_0 = 917/1,025$. The open-water dispersion relationship (black curve) is included for comparison.

The normalization in (1) is a choice that naturally follows: The candidates of length scale in the system are the water depth d, open-water wavelength $2\pi/k_{ow}$, and ice layer thickness h. The water depth d is irrelevant, since we consider the inviscid water under the ice cover to be deep (infinite). It is evident in the literature that the effects on waves depend on the ice cover thickness h (e.g., Doble et al., 2015), among other conditions. This leads to the choice of h as the scale for length. The scale for time, $\sqrt{h/g}$, follows. Of course, one could scale k using its counterpart k_{ow}. That, however, would make the length scale frequency dependent and the interpretation of dimensionless dispersion relationship less straightforward.

In dimensional analysis, the Buckingham Pi theorem can be used to determine the number of dimensionless variables/parameters that are needed to describe the original physical problem involving a certain (larger) number of dimensional variables. While the Pi theorem ensures that we can reduce the number of functions/equations in the dimensionless space, it does not inform the definitions of the dimensionless groups, or the uniqueness of the definitions. In this study, formally invoking the Pi theorem is not necessary. Since we work with the dispersion relationships of the existing theories, the dimensionless parameters should naturally emerge upon normalizing the known functions using (1). Our focus is to justify the relevance and applicability of the proposed scaling/normalization by examining (a) whether or not those dimensionless parameters are physically meaningful and consist among various theories and (b) how effective it is when we analyze the data sets in different wave and ice scales, as follows.

Mass loading model. The broken ice is treated as disconnected, noninteracting floating mass points, covering the surface of inviscid water with a surface density $\rho_{ice}h$. The theory assumes that the only forces acting on the mass points are those due to the gravity and fluid pressure at the surface. By requiring that the mass points have the same vertical velocity as that of the water surface, the collective effect of the ice-containing layer is seen to be the mass loading (due to the inertia of the floating ice "particles") on the water surface. This effect modifies the water wavelength of a given frequency but does not dissipate the wave energy. Since variations of wave speed cause wave scattering, refraction, and reflection, etc., this effect can reshape the energy spectrum of a random wave as it transmits into the ice-covered water. The dispersion relationship is given in Weitz and Keller (1950) and rewritten as $\hat{k}(\hat{\omega};\Pi_0)$; that is,

$$\hat{k} = \frac{\hat{\omega}^2}{1 - \Pi_0\hat{\omega}^2}, \tag{2}$$

where

$$\Pi_0 = \rho_{ice}/\rho \tag{3}$$

is the ratio of ice density to that of water. The inertial force (the acceleration of "mass points") of the ice layer counteracts the restoring force of gravity, leading to a wavelength shorter than $2\pi/k_{ow}$ of the same frequency. Given Π_0, the propagation of a 10-s wave under an ice layer of $h = 1$ m is similar to that of a 1-s wave under an ice layer of $h = 1$ cm, since they have the same $(\hat{\omega}, \hat{k})$. From (2), $\hat{\omega} < 1/\sqrt{\Pi_0}$. As $\hat{\omega} \to 1/\sqrt{\Pi_0}$, $\hat{k} \to \infty$ rapidly (vanishing water wavelength for a finite ice thickness); see Figure 1. This gives a maximum frequency $\omega_{max} = \sqrt{\rho g/\rho_{ice}h}$ that has a physical implication in practice: When waves from open ocean propagate toward an ice-covered region, those of frequencies close to ω_{max} will be strongly reflected (back scattering); no wave of $\omega > \omega_{max}$ can transmit into the ice-covered water. For $h = 1$ m and $\Pi_0 = 917/1025$, $f_{max} = 0.52$ Hz.

Elastic plate model. The large ice floe/sheet is treated as an elastic plate (of surface density $\rho_{ice}h$), which is nondissipative. The deformation of the thin plate is modeled following the Euler-Bernoulli beam theory (e.g., Fox & Squire, 1994). At the surface of the inviscid water under the ice cover, the continuity of normal velocity and pressure (normal stress) are required. This leads to the dispersion relationship of wave propagation on

the water covered by the thin elastic ice layer. Similar to mass loading, this effect can cause wave energy redistribution. The dispersion relationship given by Fox and Squire (1994) is rewritten as $\hat{k}(\hat{\omega}; \Pi_0, \Gamma)$; that is,

$$\hat{k} = \frac{\hat{\omega}^2}{1 - \Pi_0\hat{\omega}^2 + \frac{\Pi_0}{6(1-\nu_p)}\Gamma^2\hat{k}^4}, \tag{4}$$

where

$$\Gamma = \sqrt{G/\rho_{\text{ice}}}/\sqrt{gh} \tag{5}$$

is the elasticity parameter for the flexural-gravity waves and G is the shear modulus of solid ice. The Poission's ratio $\nu_p = 0.3$ is typical for ice (e.g., Timco & Weeks, 2010). (In Fox and Squire [1994], the Young's modulus E is used. For solids, $E = 2G(1 + \nu_p)$. Measurements of E for solid ice are typically of a few gigapascals and vary with the ice age, temperature, trapped brine volume, among other factors (Timco & Weeks, 2010). For packed broken ice (collectively being treated as a continuum plate), the effective elasticity can be much lower.) We note that $\sqrt{G/\rho_{\text{ice}}}$ is the speed of shear wave in solid ice, while $\sqrt{gh}$ is the fastest speed of surface gravity waves in fluids of depth/thickness h. The physical meaning of Γ is therefore clear: It compares the effects of elasticity and gravity, as of relevant to wave propagation. For ice sheet of $h = 1$ m and $G = 10^6$ Pa, $\Gamma \simeq 10.5$. Clearly, the effect of ice elasticity counteracts the effect of mass loading, tending to lengthen the water wavelength. For very small $\hat{\omega}$ (low wave frequency and/or thin ice), the elastic plate model is essentially same as the mass loading model; see Figure 1. From (4), the effects of mass loading and ice elasticity cancel when $\hat{\omega}^2 - \Gamma^2\hat{k}^4/6(1 - \nu_p) = 0$, at which $\hat{\omega}^2 = \hat{k}$ and the dispersion relationship curve for $\Gamma \neq 0$ intersects that for the open water. The critical frequency at the intersection is $\hat{\omega}_c = \sqrt[6]{6(1 - \nu_p)/\Gamma^2}$. For $\hat{\omega} < \hat{\omega}_c$, $\hat{k} > \hat{k}_{\text{ow}}$ due to the dominating effect of mass loading. For $\hat{\omega} > \hat{\omega}_c$, $\hat{k} < \hat{k}_{\text{ow}}$ due to the strong effect of ice elasticity. As Γ increases, $\hat{k}$ becomes significantly lower than $\hat{k}_{\text{ow}}$. When an incident wave enters the water covered by ice of strong elasticity, it must increase its wavelength so that it can propagate fast enough to exchange energy with the flexural-gravity wave in the ice, as required by the kinematic and dynamic conditions at the ice-water interface.

Viscous ice layer model. Treating the ice-containing upper layer of water as a viscous fluid having an effective viscosity much greater than that of water, Keller (1998) gave an exact solution to the vertical eigenvalue problem, obtaining the dispersion relationship for gravity waves in the two layers of fluids on a flat bed. The boundary conditions at the upper free surface are the kinematic condition concerning the vertical velocity, and zero stress vector. At the interface of the viscous ice-containing fluid and the inviscid water, the continuity of vertical velocity, normal, and tangential stresses are required. These conditions lead to a homogenous system, whose coefficient matrix (4-by-4) must have a vanishing determinant. This leads to the eigenvalue condition (the dispersion relationship) for waves in the two fluid layers. For deep water depth below the ice layer, the dimensionless dispersion equation is written as

$$\Delta(\hat{k}, \hat{\omega}; \Pi_0, R_e) = 0, \tag{6}$$

where $\Delta =$

$$\begin{vmatrix} 2\mathrm{i}\hat{k}^2 & -2\mathrm{i}\hat{k}^2 & \hat{k}^2 + \alpha^2 & \hat{k}^2 + \alpha^2 \\ 2\hat{k}^2 - \mathrm{i}R\left(\hat{\omega} + \hat{k}/\hat{\omega}\right) & 2\hat{k}^2 - \mathrm{i}R\left(\hat{\omega} - \hat{k}/\hat{\omega}\right) & -2\mathrm{i}\hat{k}\alpha - R\hat{k}/\hat{\omega} & 2\mathrm{i}\hat{k}\alpha - R\hat{k}/\hat{\omega} \\ 2\mathrm{i}\hat{k}^2 e^{\hat{k}} & -2\mathrm{i}\hat{k}^2 e^{-\hat{k}} & \left(\hat{k}^2 + \alpha^2\right)e^{\alpha} & \left(\hat{k}^2 + \alpha^2\right)e^{-\alpha} \\ \left[2\hat{k}^2 - \mathrm{i}R\left(\hat{\omega} + q\right)\right]e^{\hat{k}} & \left[2\hat{k}^2 - \mathrm{i}R\left(\hat{\omega} - q\right)\right]e^{-\hat{k}} & \left(-2\mathrm{i}\hat{k}\alpha - Rq\right)e^{\alpha} & \left(2\mathrm{i}\hat{k}\alpha - Rq\right)e^{-\alpha} \end{vmatrix}, \tag{7}$$

$$q = \frac{\hat{\omega}}{\Pi_0} - \frac{\hat{k}}{\hat{\omega}}\frac{1 - \Pi_0}{\Pi_0}, \qquad \alpha^2 = \hat{k}^2 - \mathrm{i}R, \tag{8}$$

and

$$R = h\sqrt{gh}/\nu \equiv R_e. \tag{9}$$

The Reynolds number R_e compares the inertial force to viscous force in the upper ice-agglomeration layer. Here $\sqrt{gh}$ is used to scale the fluid velocity in the upper ice layer. This is appropriate, in view of the thin

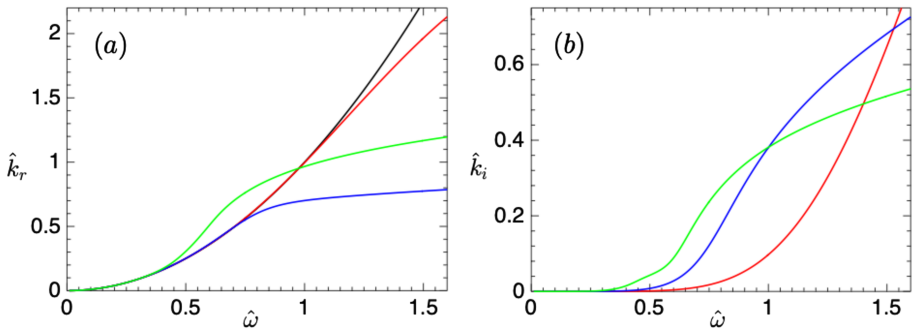

Figure 2. The dispersion relationship, that is, solutions of (6), for waves on the water covered by a viscous ice layer: (a) real wavenumber $\hat{k}_r$ as a function of $\hat{\omega}$; (b) attenuation rate $\hat{k}_i$ as a function of $\hat{\omega}$. $R_e = 30$ (red), $R_e = 3$ (blue), and $R_e = 0.3$ (green). $\Pi_0 = 917/1025$. The open-water dispersion relationship is shown in black in (a) for comparison.

ice layer, and consistent with the practice in studies of shallow water flows. The complex wavenumber $\hat{k} = \hat{k}_r + \mathrm{i}\hat{k}_i$, where $\hat{k}_r$ is the real wavenumber relating to the wave speed and $\hat{k}_i$ is the attenuation rate. The e-folding distance of wave amplitude decay is $1/\hat{k}_i$.

While the effective ice viscosity is responsible for energy dissipation, adding a small depth h of viscous fluid of nearly the same density on top of the inviscid water has two effects on the wavenumber $\hat{k}_r$. This can be understood by examining how the free surface boundary conditions for open-water waves are modified (Keller, 1998): (a) The dynamic boundary condition is changed with an additional inertial force due to the oscillation of the upper layer. This effect is similar to the mass loading on the water surface, tending to increase $\hat{k}_r$. (b) The kinematic boundary condition is changed with an additional vertical velocity due to the mass flux balance in the shallow upper layer. This second effect tends to increase the wavelength, similar to that of ice elasticity G. This similarity becomes increasingly pronounced as ν increases; compare the curves for small R_e in Figure 2a and the curves for $\Gamma \neq 0$ in Figure 1 (except for the fact that wave damping is absent from the case of elastic ice). For relatively high frequencies, wave attenuation rates can decrease with increasing ν, as the result of wavelength lengthening; see Figure 2b.

Viscoelastic ice layer model. The ice-agglomeration upper layer is modeled as a viscoelastic fluid with an effective G and ν. The effective elasticity property may come form the rigidity of ice floes of sizes that are large compared to the wavelength (Wang & Shen, 2010b). In the studies of harmonic oscillations in viscoelastic fluids, the Voigt model is usually invoked, which introduces a complex viscosity $\nu_e = \nu + \mathrm{i}G/(\rho_{\mathrm{ice}}\,\omega)$. This is for theoretical convenience, as it renders the mathematical formulation to be formally same as that for viscous fluids. Thus, Keller's (1998) solution can directly be transformed into one for linear waves on viscoelastic ice-covered water, simply by replacing the real ν with the complex ν_e. The dispersion relationship is written as

$$\Delta(\hat{k}, \hat{\omega}; \Pi_0, R_e, \Gamma) = 0, \tag{10}$$

including the effect of effective G via the definition of Γ. Here Δ is given in (7) with ν_e in place of ν in the definition of R in (9); that is,

$$R = h\sqrt{gh}/\nu_e = R_e/\left(1 + \mathrm{i}\Gamma^2 R_e/\hat{\omega}\right), \tag{11}$$

keeping the definition of R_e based on ν. The dispersion equation (10) is identical to that in Wang and Shen (2010b) who diligently worked out the expression of Δ. Such an one-line expression is not particularly elucidative, since the dispersion equation is highly implicit due to the complex expression of Δ and must be solved numerically as for (10). On the other hand, since multiplying the rows of a matrix by suitable factors will not affect the zeros of its determinant, one can improve the condition number of the 4-by-4 matrix by appropriate row normalization, hence controlling the steepness of Δ near a root. This improves the efficiency of numerical root finding.

We must note that although Γ is similarly defined as in (5) for the elastic ice plate model, the effective elasticity G is the property of the ice-agglomeration layer (which is being modeled as a viscoelastic fluid layer)

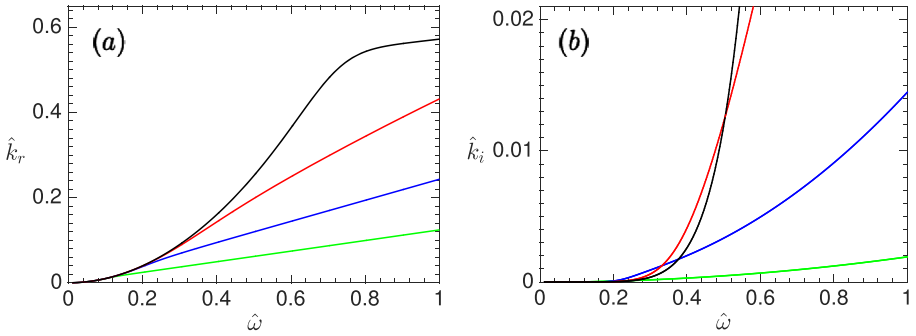

Figure 3. The dispersion relationship, that is, solutions of (10), for waves on the water covered by a viscoelastic ice layer: (a) real wavenumber $\hat{k}_r$ as a function of $\hat{\omega}$; (b) attenuation rate $\hat{k}_i$ as a function of $\hat{\omega}$. $R_e = 2$ in all cases, and $\Gamma = 1$ (red), $\Gamma = 2$ (blue), and $\Gamma = 4$ (green). The case $\Gamma = 0$ (viscous ice layer) is shown in black in (a) and (b) for easy comparison. $\Pi_0 = 917/1,025$.

and should not be taken as the shear modulus of solid ice. For Newtonian fluids (e.g., water), shear modulus is irrelevant since such fluids cannot resist any shear stress without continuous deformation (motion). Therefore, it is reasonable to expect that the effective elasticity of the composite fluid of ice-water mixture is much smaller than the shear modulus of solid ice. It should also be mentioned that the approach of treating the ice-containing upper layer as a viscoelastic fluid is different from the model of a floating viscoelastic ice plate (e.g., Bates & Shapiro, 1981). Since the dynamics of a solid plate is different from that of a fluid layer, the conditions at the ice-water interface are different. For the mathematical details of the appropriate theories, a reader is referred to Wang and Shen (2010b) and Bates and Shapiro (1981).

Given R_e and Π_0, $\hat{k}_r$ decreases with increasing Γ, as expected; see Figure 3a. For sufficiently high $\hat{\omega}$, the attenuation rate $\hat{k}_i$ decreases rapidly as Γ increases, but at low $\hat{\omega}$, $\hat{k}_i$ does not vary with Γ monotonically; see Figure 3b. In layered fluids, there are multiple modes of admissible wave oscillations, corresponding to the ways that a layer interacts with its neighboring layer(s). For example, in the simplest case of two layers of inviscid fluids of slightly different densities, for each given ω there are two wavenumbers $k_1 \ll k_2$, corresponding to two modes of oscillations in the system: For k_1, the wave on the upper surface is in-phase with the wave on the interface, while for k_2 the two waves are completely out of phase; see Lamb (1932). In the two-layer system of viscous or viscoelastic ice over inviscid water, multiple wave modes similarly exist (Keller, 1998; Wang & Shen, 2010b) although the phase relationship between the oscillations in different layers may not be as simply described as in the case of two inviscid fluids, because a phase lag can be introduced by viscous damping (and elastic response in the case of viscoelastic ice model). In Figures 2 and 3, we have presented the root whose wavenumber k_r is close to its open-water counterpart k_{ow} for the given frequency. Our interest in this root is based on the observation that when waves from open ocean propagate into the ice-covered water, the wavelengths do not change significantly (Collins et al., 2018).

3. Application to Data

We first consider the laboratory studies (Newyear & Martin, 1997; Wang & Shen, 2010a; Zhao & Shen, 2015; hereafter referred to as NM97, WS10, and ZS15, respectively). There are two tests in NM97 for grease ice, two tests in WS10 for grease/pancake ice, and three tests in ZS15 for frazil/pancake, pancake, and fragmented ice. In those studies, simultaneous measurements of wavenumber and wave attenuation rate are available. Different definitions of ice thickness were reported: The layer thickness of the ice-water mixture is referred to as the undrained value, while the equivalent solid ice thickness is referred to as the drained value. ZS15 remarked that the drained value is typically about 2/3 of the undrained value. We shall use the undrained ice thickness as it represents the thickness of the upper fluid layer.

In Figures 4a and 4b, the measurements of wavenumber k[1/m] and attenuation rate k_i[1/m] are plotted against f[Hz]. For each data set, only the data points that are close to the deep water condition ($\tanh kd \simeq 1$) are shown. Upon the normalization using the appropriate ice thickness, there is a noticeable scale collapse of the data sets, as well as the reduction of data scattering, revealing the general trends of kh and $k_i h$ as functions of $\omega(h/g)^{1/2}$; see the normalized data in Figures 4c and 4d and compare with the dimensional plots in Figures 4a and 4b. Fitting $R_e = 5.3$ for the viscous ice layer model, the theoretical predictions ($\hat{k}_r = kh$

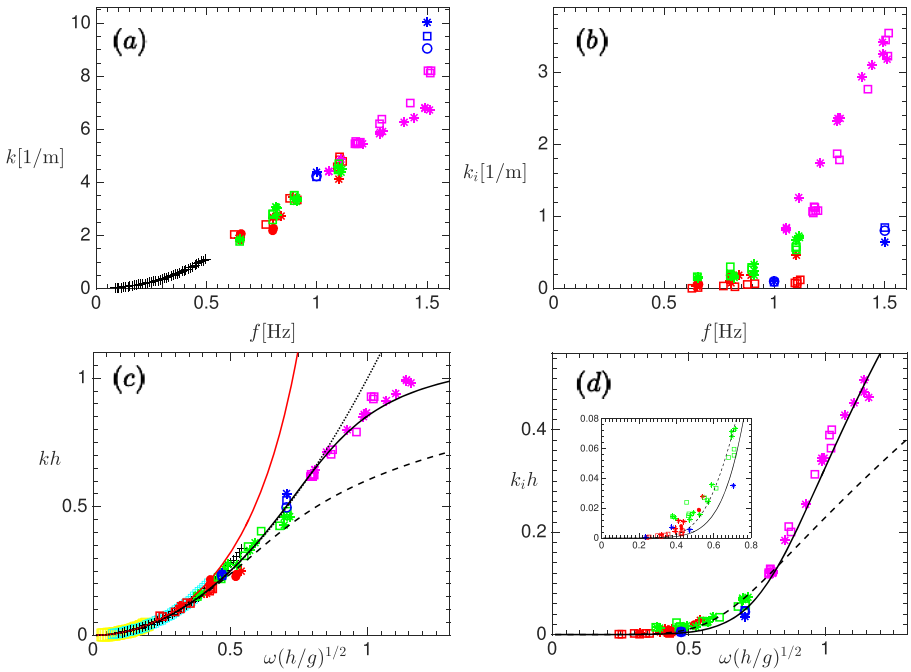

Figure 4. Lab measurements of wavenumber k[1/m] in (a) and attenuation rate k_i[1/m] in (b) as functions of f[Hz]. Symbols: magenta, two tests (h = 11.3 cm, 14.6 cm) in NM97; green, two tests (averaged h = 9.40 cm, 9.27 cm) in WS10; red, three tests (h = 3.75 cm, 6.0 cm, 10.5 cm) in ZS15; blue, the SIWI data set for grease ice (h = 5.5 cm averaging along the tank). Normalized kh in (c) and $k_i h$ in (d) as functions of $\omega(h/g)^{1/2}$. The field data set of wavenumber in Collins et al. (2018) is included in (a) for comparison (black +), and normalized in (c) using h = 4, 18, and 30 cm (yellow, cyan, and black symbols, respectively); see the text. Theoretical curves: viscous ice layer mode (black solid, R_e = 5.3); viscoelastic ice layer model (black dashed, R_e = 2.5, Γ = 0.5); in (c) the mass loading (red solid) and open-water (black dotted) dispersion relationships are included for comparison. $\Pi_0 = 917/1,025$. The inset in (d) is a zoom-in for the data of WS10 and ZS15.

and $\hat{k}_i = k_i h$) overall agree well with the normalized data, though the theory slightly underestimates the attenuation rates in WS10 and ZS15. The comparison with these latter can be improved by the viscoelastic ice layer model with $R_e = 2.5$ and $\Gamma = 0.5$, but it underestimates kh (by as much as 70%) and $k_i h$ (by as much as 160%) in the experiments of NM97.

From R_e, we can estimate the effective ice viscosity ν using the thickness h. For example, for $R_e = 5.3$, ν = 0.0224 and 0.0330m^2/s, respectively, for Tests 1 and 2 in NM 97 and fairly close to the values given in NM97. For WS10 (which reported h for every data point), we estimate the averaged $\nu = 0.0171$ and 0.0167m^2/s for the two tests. These are smaller than the values given by WS10, but of the same order of magnitude. ZS15 estimated (ν, G) by directly fitting the data in the dimensional plane and obtained (ν, G)=(0.0140m^2/s, 21.0Pa), (61.0m^2/s, 5×10^{5}Pa), and (140.0m^2/s, 10^{6}Pa) for their Tests 1, 2, and 3, respectively. For $R_e = 2.5$ and $\Gamma = 0.5$, we estimate (ν, G)=(0.0091m^2/s, 84.34Pa), (0.0184m^2/s, 134.94Pa), and (0.0426m^2/s, 236.14Pa). For Tests 2 and 3, our estimates of ν and G are of several orders of magnitude smaller than ZS15's. We do not have an explanation for the discrepancy. We note, however, that the attenuation rates in ZS15's Tests 2 and 3 are *not* of orders of magnitude greater than those in Test 1, despite the orders of magnitude differences inZS15's estimates of ν and G.

In Figure 4, we have also included a data set from a newly conducted study at the University of Melbourne's Sea-Ice-Wave Interaction (SIWI) Facility. The data set shown here is from the plane waves of 1.0-, 1.5-, and 2.0-cm amplitude that are affected by a layer of grease ice of 60% volume concentration (see supporting information, and Parra et al. [2019] and Yiew et al. [2019]) for the technical details of the experiments). Both the wavenumber and attenuation rate data are seen to fall onto the general trends of the normalized data sets mentioned above.

In field studies, simultaneous measurements of k and k_i are usually unavailable. The recent "Sea State" experiments, funded by the Office of Naval Research, provided a comprehensive study of wave attenuation

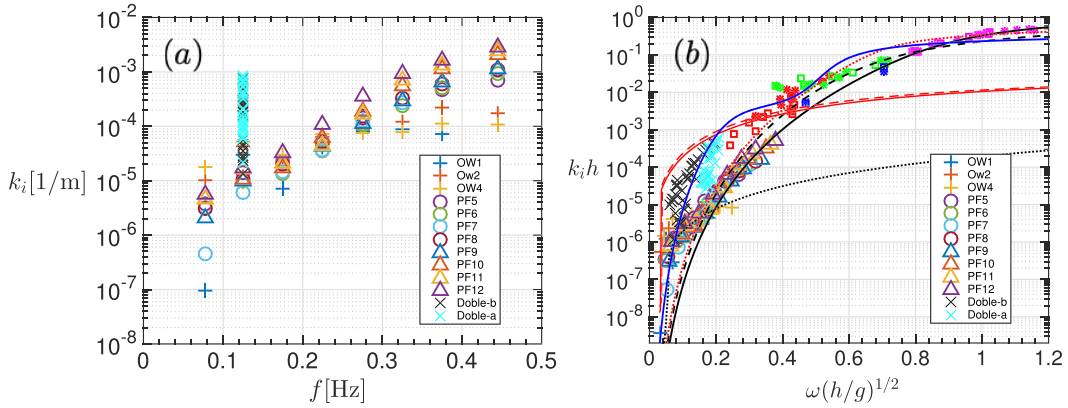

Figure 5. (a) Field data sets of k_i[1/m] versus f[Hz]: the Arctic "Sea State" experiments (symbols +, ∘, △); the data sets in Doble et al. (2015) at $f = 0.125$ Hz for the Weddell Sea (symbols ×). (b) $k_i h$ versus $\omega(h/g)^{1/2}$ (see the text for h). The smaller symbols (not included in the legend) above the field data are the lab data sets in Figure 4d. Theoretical curves: viscous ice layer model (black solid, $R_e = 5.3$; blue solid, $R_e = 0.05$); viscoelastic ice layer model (black dashed, $R_e = 2.5$, $\Gamma = 0.5$; black dotted, $R_e = 2.5$, $\Gamma = 8.0$); theoretical results using ZS15's estimates of (ν, G) for their Tests 1, 2, and 3 are shown in red (dotted, dashed, and solid, respectively).

under various conditions in the Arctic Ocean. In Figure 5a, k_i[1/m] versus f[Hz] is shown for 11 data sets from the "Sea State" study. These are from Rogers et al. (2018b), based on the model-data inversion using WAVEWATCH III® and the buoy data. The waves were in deep water (off the shelf). The alphanumeric ice codes (OW# and PF#) are the qualitative visual impression of the thickness of the pancake and frazil ice matrix based on the sorting of mosaics of photographs taken by the buoys (Rogers et al., 2016, 2018a). In general, the ice thickness for the OW-label is thinner than that for the PF-label and increases with the numeric value within a label. Estimates of ice thickness during the field experiments vary significantly but are mostly clustered around 5 to 10 cm based on the frazilometer data (Wadhams et al., 2018). Simultaneous measurements of h for the individual data sets are not available. To illustrate the influence of scaling in analyzing the data, we use a hypothetical relation between the ice code and ice thickness, assuming h to linearly increases, say, from 4 cm for OW1 to 18 cm for PF12. Doble et al. (2015) analyzed the field data in the ice region of the Weddell Sea, exploring the empirical relationship between wave attenuation and pancake/frazil ice thickness. For the peak wave period $T = 8$ s (deep water wave), they showed two sets of $(2k_i, h_{\text{eq}})$, where h_{eq} is the equivalent solid ice thickness, for the data during the compression and dilation phases of the buoy array; see Figure 2 in Doble et al. (2015). These are included in Figure 5a, labeled as "Doble-b" and "Doble-a." To estimate the undrained ice layer thickness for Doble et al.'s data, we use $h_{\text{eq}} = 0.8h$. This is based on a crude argument that solid volume fraction c is equally shared in all three dimensions; therefore, the ratio between h_{eq} and h is approximately $c^{1/3}$. Doble et al. (2015) remarked that the ice volume fractions in pancakes and frazil ice are 0.7 and 0.4, respectively. Taking the average, we estimate the ratio to be 0.8 between h_{eq} and h, which in fact is close to the ratio of 2/3 mentioned in ZS15.

In Figure 5b, the scale collapse of the data sets is clearly observed upon normalizing each using its ice thickness. The normalized lab data sets are included, tending to follow the general trend extending the field data. The theoretical curves that are used to fit the lab data in Figure 4d show very good agreement with the Arctic "Sea State" data of $\omega(h/g)^{1/2} > 0.15$, especially the prediction using the viscous ice layer model with $R_e = 5.3$. The Weddell Sea data of Doble et al. (2015) are expected to have higher attenuation rate due to the ice conditions in the region. These data can be fitted by the theoretical curve of viscous ice layer model with $R_e = 0.05$, which also fits well the Arctic "Sea State" data of low $\omega(h/g)^{1/2}$ and goes through the data of ZS15 and WS10. The effective ice elasticity can significantly reduce the attenuation rate at sufficiently high frequencies; compare Figure 3b. It is therefore not surprising that the theoretical curve of viscoelastic ice layer model with $R_e = 2.5$ and $\Gamma = 0.5$ is similar to that of viscous ice layer model with a higher $R_e = 5.3$ (lower ν). For $h = 10$ cm, we estimate $\nu = 0.0187\text{m}^2/\text{s}$ for $R_e = 5.3$, and $(\nu, G) = (0.0397\text{m}^2/\text{s}, 225.40\text{Pa})$ for $R_e = 2.5$, $\Gamma = 0.5$. With a higher $\Gamma = 8.5$ (corresponding to $G = 6.51 \times 10^4$ Pa for $h = 10$ cm) and $R_e = 2.5$, the theoretical curve can fit well the Arctic data of low $\omega(h/g)^{1/2}$ but significantly underestimates all other data sets. For Doble et al.'s (2015) data ($T = 8$ s), with $R_e = 0.05$ we can estimate ν for each data points using the reported thickness h; for the mean thickness $h = 35.0$ cm, $\nu = 13.0\text{m}^2/\text{s}$. It is open to question if there

are different regimes of wave attenuation based on the frequency and ice condition. In view of the orders of magnitude differences in the estimates of (ν, G), we have also calculated the theoretical curves using the values given in ZS15; see the red curves in Figure 5b. It is clear that the curves with very large ν and G do not fit other data sets, though they are in the range of ZS15's data sets.

While the Arctic "Sea State" experiments focused on wave attenuation, there are some wavenumber measurements. Collins et al. (2018) analyzed the data and concluded that the effect of ice on wavelength is insignificant for frequencies $f < 0.3$ Hz. Since Collins et al.'s (2018) data set (see Figure 14 in that paper) presents measurements of wavenumber rather than attenuation rate, we include it in Figures 4a and 4c, comparing with the laboratory data sets of wavenumber. Collins et al. (2018) reported that the ice layer thickness $h < 30$ cm with loose pancakes and frazil ice. Collins et al.'s 2018 wavenumber data and Rogers et al.'s attenuation rate data are from the same wave array (WA3) during the "Sea State" experiments and are roughly colocated and therefore in similar ice conditions. However, the former uses the Doble buoys, while the latter uses SWIFT buoys operated by the University of Washington (Thomson, 2012), which are equipped with cameras, required for the ice-type observation reported here (W. E. Rogers, private communication, 2019). In Figure 4c, we show the normalized wavenumber data of Collins et al. (2018) using $h = 4, 18, 30$ cm, with the first two values being the lower and upper bounds of h that we assume for the Arctic attenuation rate data in Figure 5b. Despite the uncertainty in h, the field wavenumber data set collapses onto the laboratory data sets in the normalized plane; see Figure 4c. The field and laboratory wavenumber data show that the deviation from the open-water dispersion relationship is only expected when $\omega(h/g)^{1/2}$ is large. This is physically reasonable: Given a wave frequency, the thicker the ice cover is, the greater its effect is expected on the wave. On the other hand, given an ice layer of thickness h, we expect the shorter waves to be more strongly affected than the longer ones.

4. Conclusions

From a new perspective, we reexamined the continuum-based theories of wave dispersion relationship in ice-covered waters, emphasizing the importance of appropriate scaling. Main findings are summarized, as follows. (1) Using the simple scaling based on the layer thickness of ice coverage, we can identify a set of three dimensionless parameters that quantify the *relative* importance of effects due to ice inertia (mass), effective elasticity and viscosity, hence can guide the dynamic similarity between different scales. That is, the ice-containing layers having the same values of the relevant dimensionless parameter(s) have the similar effects on waves of same dimensionless frequency. (2) When the normalization is applied to laboratory and field measurements, scale collapse of different data sets is observed, suggesting the relevance of the scaling. The reduction of data scattering in the dimensionless plane is advantageous for identifying the generalized trend, and comparing with theories. (3) From the dimensionless parameters fitting the theoretical prediction, physical parameters, such as the effective ice viscosity and elasticity, can be estimated provided the thickness of ice layer is known. Such estimates tend to be more consistent, comparing to that made by directly fitting the dimensional data.

Whereas the field measurements of effective ice viscosity and elasticity are difficult, research on observing ice thickness is becoming increasingly active with the advances in remote sensing and instrumentation (Allard et al., 2018). The finding of this study suggests an alternative to infer the effective ice properties that are needed in numerical modeling of waves in marginal ice zones. The results in this study are promising but should not be regarded as being conclusive. They merely indicate that appropriate scaling is important in the studies of wave propagation under sea ice. Other scalings, yet to be proposed, are certainly possible and may be superior. We anticipate that a broader exploration and new applications will follow.

Acknowledgments
We thank Dr. Clarence Collins and Dr. Martin J. Doble for sharing the data and anonymous reviewers for helpful comments. This research was funded by the Office of Naval Research under Program Element 0602435N. Published lab data sets used in this study were directly obtained from the appropriate papers cited. The Sea State data sets are from the cited NRL reports (https://www7320.nrlssc.navy.mil/pubs.php), with the data set describing the dependence on ice type at the website (http://www.apl.washington.edu/project/project.php?id=arctic_sea_state). For the field data sets in Collins et al. (2018) and Doble et al. (2015), a reader should contact those authors directly.

References

Allard, R. A., Farrell, S. L., Hebert, D. A., Johnston, W. F., Li, L., Kurtz, N. T., et al. (2018). Utilizing CryoSat-2 sea ice thickness to initialize a coupled ice-ocean modeling system. *Advances in Space Research*, *62*, 1265–1280. https://doi.org/10.1016/j.asr.2017.12.030

Bates, H. F., & Shapiro, L. H. (1981). Plane waves in a viscoelastic floating ice sheet. *Journal of Geophysical Research*, *86*(C5), 4269–4273. https://doi.org/10.1029/JC086iC05p04269

Cheng, S., Rogers, W. E., Thomson, J., Smith, M., Doble, M. J., Wadhams, P., et al. (2017). Calibrating a viscoelastic sea ice model for wave propagation in the Arctic fall marginal ice zone. *Journal of Geophysical Research: Oceans*, *122*, 8770–8793. https://doi.org/10.1002/2017JC013275

Collins, C., Doble, M., Loud, B., & Smith, M. (2018). Observation of surface wave dispersion in the marginal ice zone. *Journal of Geophysical Research: Oceans*, *123*, 3336–3354. https://doi.org/10.1029/2018JC013788

De Carolis, G., & Desiderio, D. (2002). Dispersion and attenuation of gravity waves in ice: a two-layer viscous fluid model with experimental data validation. *Physics Letters A*, *305*, 399–412. https://doi.org/10.1016/S0375-9601(02)01503-7

Doble, M., De Carolis, G., Meylan, M. H., Bidlot, J.-R., & Wadhams, P. (2015). Relating wave attenuation to pancake ice thickness, using field measurements and model results. *Geophysical Research Letters*, *42*, 4473–4481. https://doi.org/10.1002/2015GL063628

Fox, C., & Squire, V. A. (1994). On the oblique reflexion and transmission of ocean waves from shore fast sea ice. *Philosophical Transactions of the Royal Society London A*, *347*, 185–218. https://doi.org/10.1098/rsta.1994.0044

Hayes, D. R., Jenkins, A., & McPhail, S. (2007). Autonomous underwater vehicle measurements of surface wave decay and directional spectra in the marginal sea ice zone. *Journal of Physical Oceanography*, *37*, 71–83.

Keller, J. B. (1998). Gravity waves on ice-covered water. *Journal of Geophysical Research*, *103*(C4), 7663–7669. https://doi.org/10.1029/97JC02966

Lamb, H. (1932). *Hydrodynamics*: Cambridge University Press.

Meylan, M. H., Bennetts, L. G., & Kohout, A. L. (2014). In situ measurements and analysis of ocean waves in the Antarctic marginal ice zone. *Geophysical Research Letters*, *41*, 5046–5051. https://doi.org/10.1002/2014GL060809

Meylan, M. H., Bennetts, L. G., Mosig, J. E. M., Rogers, W. E., Doble, M. J., & Peter, M. A. (2018). Dispersion relationships, power laws, and energy loss for waves in the marginal ice zone. *Journal of Geophysical Research: Oceans*, *123*, 3322–3335. https://doi.org/10.1002/2018JC013776

Mosig, J. E. M., Montiel, F., & Squire, V. A. (2015). Comparison of viscoelastic-type models for ocean wave attenuation in ice-covered seas. *Journal of Geophysical Research: Oceans*, *120*, 6072–6090. https://doi.org/10.1002/2015JC010881

Newyear, K., & Martin, S. (1997). A comparison of theory and laboratory measurements of wave propagation and attenuation in grease ice. *Journal of Geophysical Research*, *102*(C11), 25,091–25,099. https://doi.org/10.1029/97JC02091

Parra, S. M., Sree, D. K. K., Wang, D. W., Rogers, E. W., & Alexander, A. V. (2019). Experimental study on surface wave modifications by different ice covers. In *review with Cold Reg. Sci. Technol.*

Rogers, W. E., Meylan, M. H., & Kohout, A. L. (2018b). Frequency distribution of dissipation of energy of ocean waves by sea ice using data from Wave Array 3 of the ONR "Sea State" field experiment (NRL Memorandum Report. NRL/MR/7320-18-9801): Naval Research Laboratory, Stennis Space Center. MS. 25pp. ww7320.nrlssc.navy.mil/pubs.php

Rogers, W. E., Posey, G. P., Li, L., & Allard, R. A. (2018a). Forecasting and hindcasting waves in and near the marginal ice zone: Wave modeling and the ONR "Se State" field experiment (NRL Memorandum Report. NRL/MR/7320-18-9786.): Naval Research Laboratory. Stennis Space Center, MS. 179pp. ww7320.nrlssc.navy.mil/pubs.php

Rogers, W. E., Thomson, J., Shen, H. H., Doble, M. J., Wadhams, P., & Cheng, S. (2016). Dissipation of wind waves by pancake and frazil ice in the autumn Beaufort Sea. *Journal of Geophysical Research: Oceans*, *121*, 7991–8007. https://doi.org/10.1002/2016JC012251

Squire, V. A. (2007). Of ocean waves and sea-ice revisited. *Cold Regions Science and Technology*, *49*, 110–133.

Squire, V. A., Dugan, J. P., Wadhams, P., Rottier, P. J., & Liu, A. K. (1995). Of ocean waves and sea-ice. *Annual Review of Fluid Mechanics*, *27*, 115–168.

The WAVEWATCH III Development Group (2016). User manual and system documentation of WAVEWATCH III® version 5.16 (*Tech. Note 329*): NOAA/NWS/NCEP/MMAB, College Park, MD. USA, 326 pp. + Appendices.

Thomson, J. (2012). Wave breaking dissipation observed with SWIFT drifters. *Journal of Atmospheric and Oceanic Technology*, *29*, 1866–1882.

Timco, G. W., & Weeks, W. F. (2010). A review of the engineering properties of sea ice. *Cold Regions Science and Technology*, *60*, 107–129.

Wadhams, P., Aulicino, G., Parmiggiani, F., Persson, P. O. G., & Holt, B. (2018). Pancake ice thickness mapping in the Beaufort Sea from wave dispersion observed in SAR imagery. *Journal of Geophysical Research: Oceans*, *123*, 2213–2237. https://doi.org/10.1002/2017JC013003

Wadhams, P., Squire, V. A., Goodman, D. J., Cowan, A. M., & Moore, S. C. (1988). The attenuation rates of ocean waves in the marginal ice zone. *Journal of Geophysical Research*, *93*(C6), 6799–6818. https://doi.org/10.1029/JC093iC06p06799

Wang, R., & Shen, H. H. (2010a). Experimental study on surface wave propagating through a grease-pancake ice mixture. *Cold Regions Science and Technology*, *61*, 90–96.

Wang, R., & Shen, H. H. (2010b). Gravity wave propagating into an ice-covered ocean: A viscoelastic model. *Journal of Geophysical Research: Oceans*, *115*, C06024. https://doi.org/10.1029/2009JC005591

Weber, J. E. (1987). Wave attenuation and wave drift in the marginal ice zone. *Journal of Physical Oceanography*, *17*, 2351–2361.

Weitz, M., & Keller, J. B. (1950). Reflection of water waves from floating ice in water of finite depth. *Communications on Pure and Applied Mathematics*, *3*(3), 305–318.

Yiew, L. J., Parra, S. M., Wang, D. W., Sree, D. K. K., Babanin, A. V., & Law, A. W.-K. (2019). Wave attenuation and dispersion due to floating ice covers. *Applied Ocean Research*, *87*, 256–263.

Zhao, X., & Shen, H. H. (2015). Wave propagating in frazil/pancake, pancake, and fragmented ice covers. *Cold Regions Science and Technology*, *113*, 71–80.